Available online at www.sciencedirect.com
SCIENCE DIRECT®
International Journal of Heat and Mass Transfer 47 (2004) 1275–1288
International Journal of HEAT and MASS TRANSFER
www.elsevier.com/locate/ijhmt

Investigation of interfacial behavior during the flow boiling CHF transient

Hui Zhang [a], Issam Mudawar [a,*], Mohammad M. Hasan [b]

[a] *Boiling and Two-phase Flow Laboratory, School of Mechanical Engineering, Purdue University, Mechanical Engineering Building, West Lafayette, IN 47907-1288, USA*

[b] *NASA Glenn Research Center, 21000 Brookpark Road, Cleveland, OH 44135, USA*

Received 6 March 2003; received in revised form 6 September 2003

Abstract

Vertical upflow boiling experiments were performed in pursuit of identifying the trigger mechanism for subcooled flow boiling critical heat flux (CHF). While virtually all prior studies on flow boiling CHF concern the prediction or measurement of conditions that lead to CHF, this study is focused on events that take place during the CHF transient. High-speed video imaging and photomicrographic techniques were used to record the transient behavior of interfacial features from the last steady-state power level before CHF until the moment of power cut-off following CHF. The video records show the development of a wavy vapor layer which propagates along the heated wall, permitting cooling prior to CHF only in wetting fronts corresponding to the wave troughs. Image analysis software was developed to estimate void fraction from the individual video images. The void fraction records for subcooled flow boiling show the CHF transient is accompanied by gradual lift-off of wetting fronts culminating in some maximum vapor layer mean thickness, following which the vapor layer begins to thin down as the transition to film boiling ensues. This study proves the interfacial lift-off model, which has been validated for near-saturated flow boiling CHF, is equally valid for subcooled conditions.

Keywords: Critical heat flux; Flow boiling

1. Introduction

The trigger mechanism for critical heat flux (CHF) in flow boiling has been the subject of intense debate for over five decades. There is nothing approaching a unified comprehensive understanding despite the thousands of experiments conducted to date [1]. Direct observation of vapor formations near the heated wall is the most popular and effective means for gaining insight into the physical CHF trigger mechanism. Yet such techniques are often costly, time consuming and prone to failure due to the extreme temperatures encountered at CHF. This explains why flow visualization studies of the CHF mechanism tend to be qualitative, and intended mostly to develop a correlation applicable to a particular system or flow pattern. This type of experiment does little to aid the theoretical understanding of the problem.

Dryout is one type of CHF, which occurs in low mass velocities, low subcooling and/or large length-to-diameter ratio channels. It constitutes a relatively mild form of CHF and is associated with relatively small excursions in the wall temperature. *Departure from nucleate boiling* is a far more severe form of CHF because it precipitates abrupt rise in the wall temperature even in the presence of abundant liquid flow in the channel core. The present study concern this more severe type of CHF, which is of vital importance to the design and safety assessment of nuclear, aerospace, defense, medical and electronic systems involving intense heat removal from heat-flux-controlled surfaces.

* Corresponding author. Tel.: +1-765-494-5705; fax: +1-765-494-0539.
E-mail address: mudawar@ecn.purdue.edu (I. Mudawar).

0017-9310/$ - see front matter © 2003 Elsevier Ltd. All rights reserved.
doi:10.1016/j.ijheatmasstransfer.2003.09.014

Nomenclature

b	ratio of wetting front length to wavelength, w/λ
c	wave speed
$c_{p,f}$	specific heat of liquid
g_e	earth's gravitational acceleration
h_{fg}	latent heat of vaporization
H_k	height (thickness) of phase k layer
k	wave number, $2\pi/\lambda$
k_c	critical wave number, $2\pi/\lambda_c$
P	pressure
q''	wall heat flux
q''_m	critical heat flux
q''_w	wetting front lift-off heat flux
t	time
T	temperature
$\Delta T_{sub,i}$	inlet subcooling, $T_{sat,i} - T_{b,i}$
$\Delta T_{sub,o}$	calculated outlet subcooling, $T_{sat,o} - T_{b,o}$
U	mean liquid inlet velocity
U_f	liquid phase velocity
U_g	vapor phase velocity
$U_{g,n}$	vapor velocity in wetting front normal to wall
w	wetting front length used in CHF model
z	streamwise coordinate
z^*	extent of continuous upstream wetting region
z_0	streamwise distance where $U_f = U_g$

Greek symbols

α	void fraction
δ	mean vapor layer thickness; vapor layer amplitude used in CHF model
η	interfacial perturbation
η_0	amplitude of interfacial perturbation, $\eta_0 = \delta$
θ	flow orientation angle
λ	vapor layer wavelength
λ_c	critical wavelength
ρ	density
ρ''_f	modified liquid density
ρ''_g	modified vapor density
σ	surface tension

Subscripts

b	bulk liquid
c	critical
f	saturated liquid
g	saturated vapor
i	inlet
m	maximum, critical heat flux
o	outlet
sat	saturation
w	wall

Other than dryout, four major physical mechanisms have been postulated as the trigger for CHF in subcooled and near-saturated flow boiling. All these mechanisms are based upon some physical process that restricts bulk liquid flow from reaching the heated wall.

1.1. Boundary layer separation model

The earliest subcooled CHF model is based on the hypothesis of boundary layer separation. As illustrated in Fig. 1(a), the forward movement of near-wall liquid in the boundary layer is obstructed by vapor production at the wall. At CHF, this obstruction decreases the near-wall liquid velocity gradient to the point of liquid stagnation just outside the bubble layer. This greatly decreases the liquid's ability to compensate for the intense vapor production at the wall. Eventually, the bulk liquid flow detaches from the heated wall, inducing dryout downstream.

Kutateladze and Leont'ev [2] postulated vapor production in flow boiling is very similar to gas injection into a turbulent boundary layer flowing over a permeable flat plate. To predict subcooled CHF, they utilized a pool boiling CHF correlation and a subcooling parameter which accounted for the heat flux necessary to induce boundary layer separation. However, boundary layer separation and pool boiling are two distinctly different processes and there is no physical reason to expect that their heat fluxes are in any way additive. Tong [3,4] and Purcupile and Gouse Jr.[5] developed empirical CHF correlations loosely built upon the boundary layer separation model.

1.2. Bubble crowding model

A second mechanism that has been postulated to trigger CHF is bubble crowding. This mechanism is governed by turbulent fluctuations in the liquid flow at the outer edge of the near-wall bubbly layer. As illustrated in Fig. 1(b), these turbulent fluctuations become too weak at high heat fluxes to transport bulk liquid through the dense bubbly layer in order to cool the wall.

To model this process, a critical void fraction that precedes CHF must be defined. It is the maximum volume fraction at which the bubbles can maintain separation in the bubbly layer with no significant contact. The bubbly layer was idealized by Weisman and Pei [6] as consisting of ellipsoidal bubbles having an axis ratio

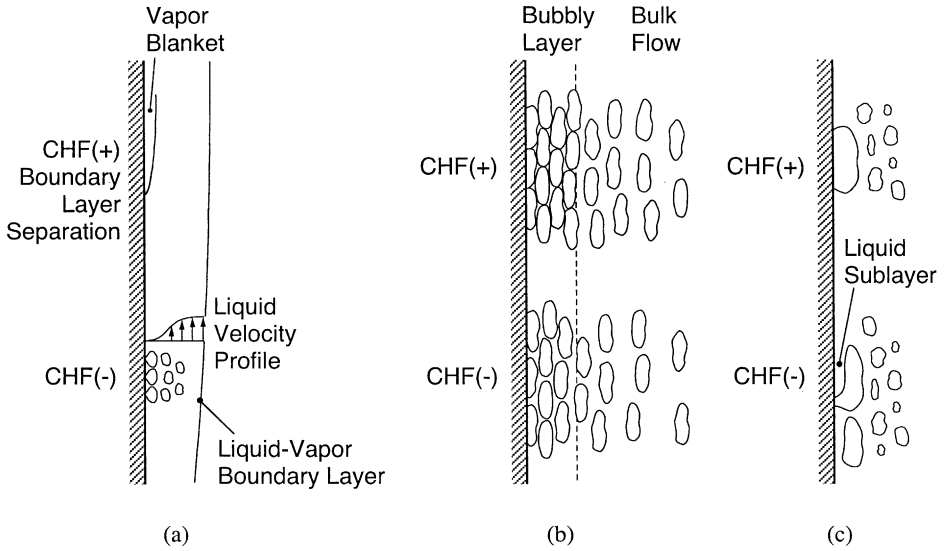

Fig. 1. Flow boiling CHF mechanism according to (a) boundary layer separation model, (b) bubble crowding model and (c) sublayer dryout model.

of 3–1. When these idealized bubbles are stacked into a bubbly layer they produce a near-wall void fraction of 82%. Weisman and Pei utilized three empirical parameters to achieve good agreement with CHF data for water. Their model also showed good predictions for R-11, R-113, liquid nitrogen and anhydrous ammonia and was later extended by Weisman and Ileslamlou [7] to highly subcooled conditions.

Overall, the use of several empirical constants and, more importantly, the critical void fraction assumption raise serious questions about the validity of this model. Depending on flow conditions, Styrikovich et al. [8] measured near-wall void fractions from 30% to 95%, which contradicts the fixed value of 82% adopted in the bubble crowding model.

1.3. Sublayer dryout model

The third type of CHF trigger mechanism is based upon sublayer dryout. The sublayer dryout model treats the liquid–vapor exchange as a more localized phenomenon than the boundary layer separation model and bubble crowding model do. The sublayer dryout model is based on observations from a number of earlier studies. Several researchers reported observing significant coalescence of small vapor bubbles at high heat fluxes into vapor patches that moved along the heated wall. Furthermore, the vapor patches were observed to trap a thin liquid sublayer which seemed to provide the necessary cooling for the wall prior to CHF [9–12].

The sublayer dryout model is based on the assumption that CHF will commence upon evaporation of the thin liquid sublayer. Lee and Mudawar [13] provided the basic framework for this model. As depicted in Fig. 1(c), they postulated CHF to occur when the wall heat flux surpasses the enthalpy of liquid replenishing the sublayer from the bubbly layer and bulk liquid. The Helmholtz wavelength, calculated from bubble rise velocity and liquid velocity, was used to determine the length of the sublayer since bubbles that are longer than the Helmholtz wavelength are unstable and should break up into smaller bubbles.

Several researchers borrowed much of the original formulation of the Lee and Mudawar model. Lin et al. [14] modified this model slightly to aid the prediction of CHF in both subcooled and low positive quality flows. The Katto [15–17] and Celata et al. [18,19] CHF models are all fairly similar to the Lee and Mudawar model. The significant differences in these models are found in the methods used to calculate vapor velocity and liquid sublayer thickness.

1.4. Interfacial lift-off model

The fourth CHF mechanism is based upon the interfacial lift-off model. This model was developed by Galloway and Mudawar [20,21] based upon extensive flow visualization experiments they carried out at near-saturated conditions, relatively low flow velocities and a heated length 4.96 times the hydraulic diameter. Using back lighting of the boiling flow in a rectangular channel with transparent sidewalls, they were able to clearly capture the liquid–vapor interface as a silhouette. As CHF was approached, a series of vapor patches were observed to propagate along the heated wall resembling a fairly continuous wavy vapor layer. As illustrated in

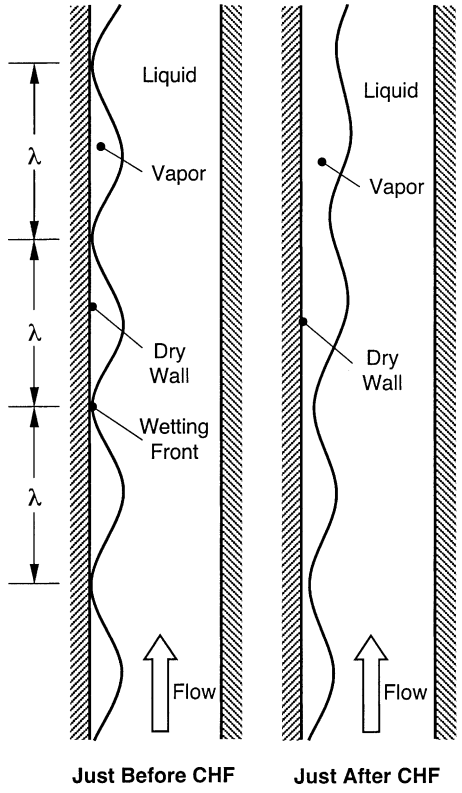

Fig. 2. Flow boiling CHF mechanism according to interfacial lift-off model.

Fig. 2, the vapor patches appeared to insulate the heated wall beneath and virtually all the wall cooling occurred by vigorous boiling in *wetting fronts* located in troughs between the vapor patches. They identified the CHF trigger mechanism by separation of the most upstream wetting front off the wall. Once this cooling path was eliminated, the heat flux increased in the other wetting fronts, forcing them to separate in succession and leading to the formation of a continuous vapor blanket which insulated the entire heated wall. Galloway and Mudawar postulated wetting fronts detach when the pressure force associated with interfacial curvature, which is responsible for maintaining liquid contact with the wall, is overcome by vapor momentum in the wetting front normal to the heated wall.

The interfacial lift-off model was extended by Gersey and Mudawar [22,23] to a wider channel and heated lengths up to 16.5 the hydraulic diameter. Sturgis and Mudawar [24,25] performed flow visualization on long heaters for both saturated and subcooled conditions. The wavy vapor patches observed at saturated conditions by Galloway and Mudawar, and Gersey and Mudawar were the dominant vapor formations in subcooled flow as well. Compared with saturated conditions, both wavelength and amplitude of the vapor patches decreased with increased subcooling. Sturgis and Mudawar also performed a statistical investigation of vapor formations and categorized them into ones that involved trapping of a liquid sublayer (as described by the sublayer dryout model) versus those that followed the wavy vapor layer depiction. The vapor formations necessary for sublayer dryout were observed less than 10% of the time for near-saturated flow and about 25% for subcooled flow, proving the wavy vapor layer behavior occurs with far greater frequency.

Zhang et al. [26,27] investigated the effects of gravitational force on flow boiling CHF using different flow orientations. They identified six different CHF regimes associated with the different orientations, flow velocities and subcoolings. Vertical upflow at all velocities, as well as high velocity flow (>0.5 m/s) at all orientations was dominated by the wavy vapor layer behavior. They observed that the vapor waves generated upstream tend to preserve a wave curvature value as they propagate along the heated wall and confirmed that CHF is triggered by lift-off of vapor waves with a certain wave curvature value. They modified the interfacial lift-off model to incorporate the effects of gravitational force on near-saturated flow boiling CHF.

Pursuit of the trigger mechanism for flow boiling CHF has thus far taken the form of photographic study of interfacial behavior at conditions just preceding the occurrence of CHF. Researchers often refrain from investigating events that take place as the wall temperature begins to escalate when CHF ensues due to obvious concerns over potential damage to the flow channel that may accompany this temperature excursion. Water flow boiling CHF experiments are especially prone to permanent damage given both the large magnitude of CHF and fast temperature excursion for most operating conditions.

The primary objective of the present study is to track interfacial behavior *during the CHF transient*. Using FC-72, which has a relatively low boiling point and low CHF, the temperature excursion is both mild and slow compared to water, giving the operator adequate time to track the development of near-wall vapor formations. The transient behavior of these formations is used to both confirm the interfacial lift-off model as well as develop a clear understanding of what happens during this most dangerous phenomenon in a flow boiling system.

Another key goal of this study is to assess the validity of the interfacial lift-off mechanism to subcooled conditions since prior efforts have been focused on validation only for near-saturated conditions.

2. Basic formulation of interfacial lift-off model

Since the interfacial lift-off model has been adequately explained in several of the studies cited in the

previous section, only the basic equations describing the model development and are important to the present study, are provided here.

The flow visualization studies by Zhang et al. [26,27] captured a wavy liquid–vapor interface that developed along the heated wall and permitted liquid contact with the wall only in discrete wetting fronts as illustrated as Fig. 2. Heat appeared to be transferred to the liquid by means of vigorous boiling only in the wetting fronts.

Interfacial contact with the heated wall prior to CHF dictates that the interfacial wavelength must exceed a critical wavelength given by

$$k_c = \frac{2\pi}{\lambda_c} = \frac{\rho_f'' \rho_g'' (U_g - U_f)^2}{2\sigma(\rho_f'' + \rho_g'')} + \sqrt{\left[\frac{\rho_f'' \rho_g'' (U_g - U_f)^2}{2\sigma(\rho_f'' + \rho_g'')}\right]^2 + \frac{(\rho_f - \rho_g) g_e \cos\theta}{\sigma}}, \quad (1)$$

where $\rho_f'' = \rho_f \coth(kH_f)$ and $\rho_g'' = \rho_g \coth(kH_g)$ and $g_e \cos\theta$ is the component of gravity perpendicular to the heated wall. A large velocity difference between the two phases serves to destabilize the interface while surface tension helps maintain interfacial stability. Body force plays a far more complex role and can be stabilizing or destabilizing depending on orientation relative to gravity.

Within the wetting fronts, the momentum associated with vapor effusion tends to push the interface away from the heated wall. The momentum is resisted by a pressure force that is induced by interfacial curvature. The relative magnitude of those two opposing effects dictates whether or not liquid will be able to reach the wall. When the vapor momentum exceeds the pressure force, the interface will be lifted away from the wall and any cooling provided by the wetting front is lost. Heat that would otherwise be dissipated within the lifted wetting front is channeled to neighboring wetting fronts, increasing heat flux in those wetting fronts. The ensuing increase in vapor momentum in those wetting fronts creates conditions that are even more conducive to interfacial lift-off. A chain reaction begins to propagate along the heated wall, lifting wetting fronts in succession and depriving the wall from liquid access.

Using classical instability theory, the pressure difference resulting from a small disturbance, $\eta(z,t) = \eta_0 e^{ik(z-ct)}$, perpendicular to the interface can be expressed as

$$P_f - P_g = -\left[\rho_f''(c - U_f)^2 + \rho_g''(c - U_g)^2 + (\rho_f - \rho_g)\frac{g_n}{k}\right] k\eta_0 e^{ik(z-ct)}. \quad (2)$$

The pressure force along the wetting front is obtained by integrating Eq. (2) over a length $b\lambda$ centered at the wetting front:

$$\overline{P_f - P_g} = \frac{4\pi\sigma\delta}{b\lambda^2}\sin(b\pi), \quad (3)$$

where b is the wetting front length to wavelength ratio and δ the local mean vapor layer thickness.

The local heat flux required to lift the interface away from the wall is determined by equating the vapor momentum in the wetting front normal to the wall, $\rho_g U_{g,n}^2$, to the pressure force:

$$q_w'' = \rho_g(c_{p,f}\Delta T_{sub,i} + h_{fg})\sqrt{\frac{\overline{P_f - P_g}}{\rho_g}} = \rho_g(c_{p,f}\Delta T_{sub,i} + h_{fg})\left[\frac{4\pi\sigma}{\rho_g}\frac{\sin(b\pi)}{b}\right]^{1/2}\frac{\delta^{1/2}}{\lambda}. \quad (4)$$

Eq. (4) shows the lift-off heat flux, q_w'', is proportional to $\delta^{1/2}\lambda$, which is a measure of interfacial curvature.

Flow visualization experiments by Zhang et al. revealed the existence of a continuous wetting region near the leading edge of the heated wall, whose length, z^*, can be expressed as

$$z^* = z_0 + \lambda_c(z^*), \quad (5)$$

where z_0 is the distance from the leading edge to the location where the vapor velocity just exceeds the liquid velocity. Eq. (5) implies the interfacial waves are first formed at z^*, downstream from which the wavy vapor layer begins to propagate along the heated wall.

The curvature parameter $\delta^{1/2}\lambda$ in Eq. (4) was calculated by Zhang et al. from measurements of the wavy layer interfacial features. These measurements revealed the majority of $\delta^{1/2}\lambda$ values in both the middle and outlet sections of the heated wall range from $0.5(\delta^{1/2}\lambda_c)$ to $1.5(\delta^{1/2}\lambda_c)$, where both δ and λ_c are calculated at z^*. This implies the interfacial waves generated upstream at z^* preserve their curvature as they travel along the heated wall. The same measurements also revealed that, while the wetting front length increases in the flow direction, it remains a fairly constant fraction of the local wavelength, $w = b\lambda$, where $b = 0.2$. Since CHF is defined as the average heat flux over the entire heated wall, Eq. (4) can be simplified as

$$q_m'' = \rho_g(c_{p,f}\Delta T_{sub,i} + h_{fg})\left[\frac{4\pi\sigma b\sin(b\pi)}{\rho_g}\right]^{1/2}\left.\frac{\delta^{1/2}}{\lambda_c}\right|_{z^*}, \quad (6)$$

where both δ and λ_c are calculated at z^* using a separated two-phase flow model [26,27].

It is important to emphasize that the interfacial lift-off model has never been systematically validated for subcooled conditions. Two key obstacles to

accomplishing this validation are (a) the difficulty of determining the partitioning of wall heat flux between sensible and latent heat transfer to the fluid and (b) the extreme difficulty of capturing and characterizing the small interfacial features prevalent in subcooled flow. The present study aims to better characterize those small interfacial features to confirm the interfacial lift-off mechanism for subcooled flow boiling.

3. Heat transfer measurements

The flow boiling test module for this study was fabricated to enable side viewing of vapor effusion and coalescence along a heated wall. The module was formed by clamping together two plates of transparent polycarbonate plastic (Lexan). As shown in Fig. 3, the flow channel itself was formed by milling a 5.0 mm × 2.5 mm rectangular slot into the bottom plate of the test module. A portion of the bottom plate was milled out and a heating block inserted flush with one side of the flow channel. Fluid temperature and pressure were measured through access taps in the cover plate (not shown in Fig. 3) both upstream and downstream of the heated wall.

The heating block was fabricated from oxygen-free (high-purity) copper. Heat was supplied by high-power-density cartridge heaters that were embedded in the thick section of the copper block. The heat was channeled into a thinner portion having the same thickness as the flow channel. The heated wall of the flow channel consisted of the edge of the thin section of the heating block, which was 101.6 mm long and 2.5 mm wide.

Five arrays of Type-K (Chromel–Alumel) thermocouples were inserted strategically along the thin section of the heating block. Each thermocouple array consisted of three thermocouples embedded 1.02, 6.10, and 11.18 mm from the wetted wall. A linear curve fit to the thermocouple readings in each array yielded a temperature gradient perpendicular to the wall that was used to calculate both local heat flux, q'' and local wall temperature, T_w, with 7.9% and 0.3 °C uncertainty, respectively.

Fig. 4 shows the main components of a closed two-phase flow loop that was used to supply liquid FC-72 to the test module and condition it to desired operating conditions.

4. Heat transfer results

Experiments were performed in the vertical upflow orientation for outlet subcoolings of $\Delta T_{sub,o} = 3$ and 30 °C, outlet pressure of 138 kPa and velocities up to 1.5 m/s. Each test yielded a boiling curve, up to and in-

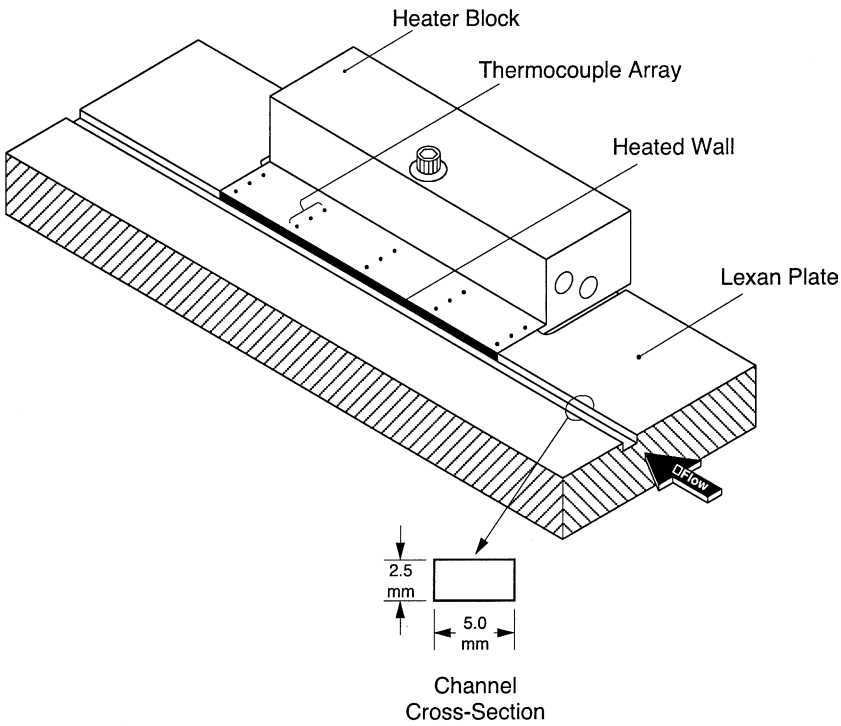

Fig. 3. Heater inserted into bottom plate of test module.

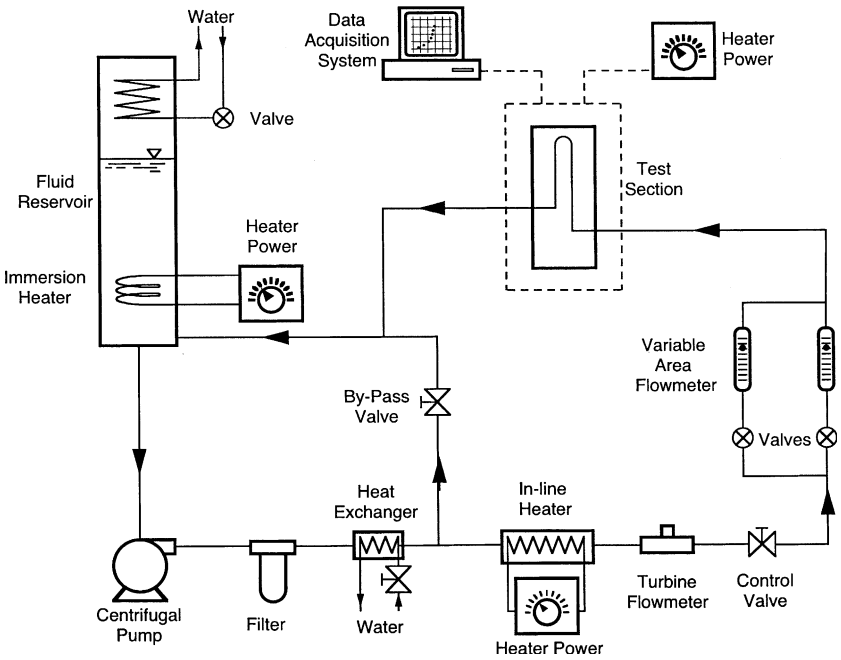

Fig. 4. Two-phase flow loop.

cluding the CHF point. CHF was detected by a sudden decrease in the temperature gradient measured by the downstream thermocouple array and an increase in wall temperature at the same location.

Fig. 5(a) shows boiling curves at $\Delta T_{sub,o} = 3$ °C for $U = 0.5$, 1.0 and 1.5 m/s. The heat flux at the location of the downstream thermocouple array is plotted against the difference between the wall temperature and bulk temperature at the same axial location. The bulk temperature was calculated from the measured channel inlet temperature and total heat added to the fluid up to the downstream thermocouple location. The three curves in Fig. 5(a) exhibit typical trends with increase velocity: upward shift in the single-phase liquid regime followed by merging of data for different velocities in the nucleate boiling regime and culminating in increasing CHF values with increasing velocity. Similar trends are shown in Fig. 5(b) for $\Delta T_{sub,o} = 30$ °C, except that temperature differences are greater due to much lower T_b values for about the same T_w as for $\Delta T_{sub,o} = 3$ °C.

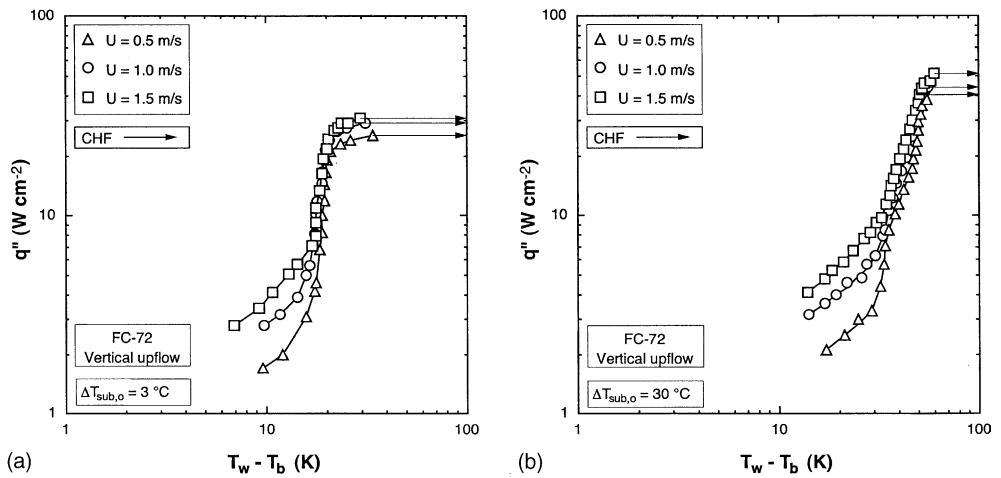

Fig. 5. Effects of velocity on boiling curve for (a) $\Delta T_{sub,o} = 3$ °C and (b) $\Delta T_{sub,o} = 30$ °C.

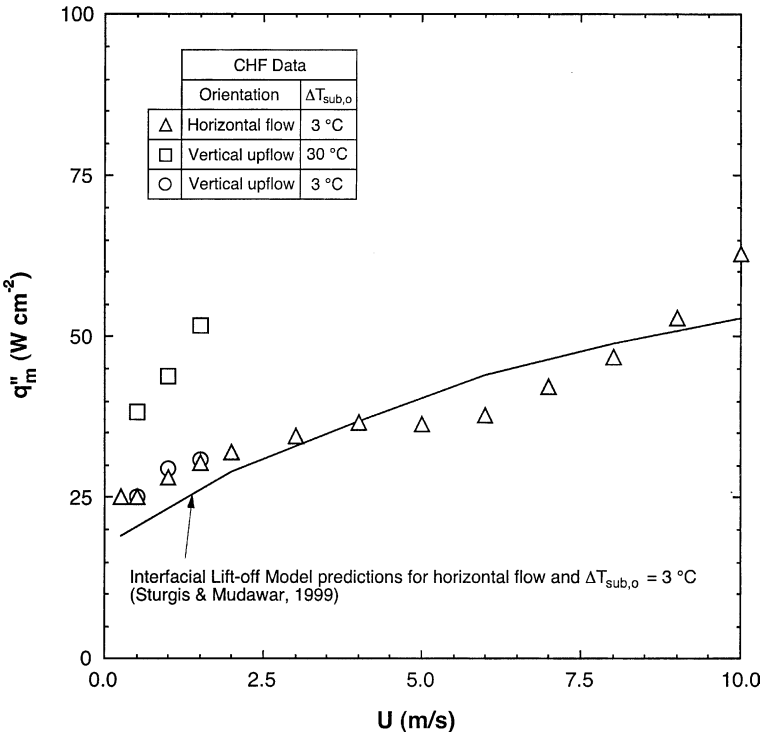

Fig. 6. Comparison of predicted and measured CHF.

Fig. 6 shows CHF increases with increasing flow velocity for each of the two subcooling levels tested. The higher subcooling provides an appreciable increase in CHF because of the fluid's capacity to absorb more of the supplied heat in the form of sensible energy, as well as the added benefit of reducing the size of vapor masses near the wall by condensation. Also shown in Fig. 6 are both the near-saturated horizontal flow boiling CHF data and corresponding interfacial lift-off model predictions of Sturgis and Mudawar [25].

5. Void fraction estimation

5.1. Flow visualization techniques

A Redlake MotionScope PCI 8000 S high-speed digital video system was used to capture the interfacial features. The electronic shutter for this system can be modulated from 1/60th s down to 10 μs depending on the frame rate and the amount of light available to "freeze" the liquid–vapor interface. After attempting different frame rates, a rate of 1000 frames/s was deemed very suitable for the conditions of the present study. At this frame rate, the system's recording capacity was limited to just over 2 s of video, which consisted of 2034 individual frames. This recording time was far too short to capture the detailed CHF transient. Therefore, the system was modified for the transient CHF experiments by connecting a canon GL1 digital video camera to the Redlake MotionScope video system. This Redlake MotionScope video system provided a shutter speed of 1/20,000 s needed to freeze the interfacial features, while the Canon video camera recorded images at a rate of 29.97 frames/s.

Fig. 7 shows the flow visualization setup. The digital video camera was positioned perpendicular to the flow channel. The camera was attached to a tripod so that it could traverse the entire vertical length of the heated wall. This was necessary because the video segments were taken at the inlet, middle and outlet of the heated wall separately in order to capture the streamwise development of interfacial features with high resolution. The flow was backlit with a light source with adjustable intensity and focus. A semi-opaque sheet of paper was used to soften and diffuse the incoming light. Like the camera, the light source was mounted on a tripod to traverse the entire length of the heated wall.

Fig. 8 shows a composite of flow characteristics at $U = 1.5$ m/s captured just prior to CHF at the inlet, middle and outlet sections of the heated wall. For $\Delta T_{sub,o} = 3$ °C, Fig. 8(a), the vapor flow takes the form of relatively long, periodic wavy vapor patches separated by liquid wetting fronts. At the channel exit, the

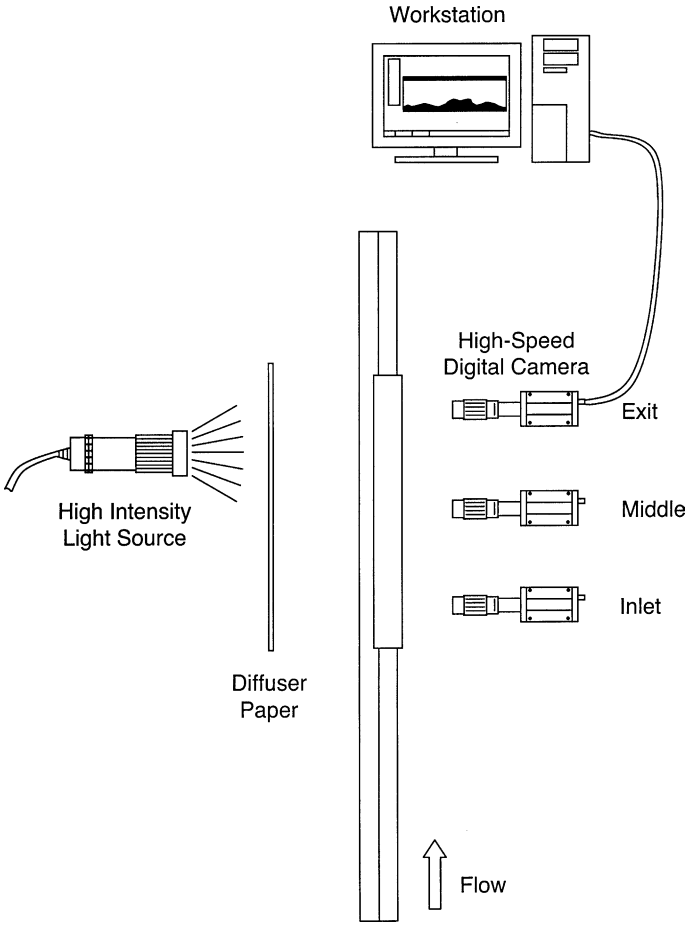

Fig. 7. Flow visualization setup.

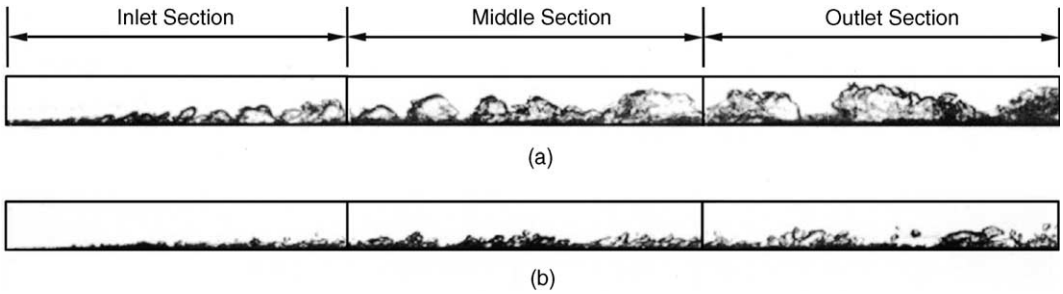

Fig. 8. Composite images of wavy vapor layer in vertical upflow at $U = 1.5$ m/s just prior to CHF for (a) $\Delta T_{sub,o} = 3$ °C and (b) $\Delta T_{sub,o} = 30$ °C.

vapor layer occupies a large fraction the channel cross-section. For $\Delta T_{sub,o} = 30$ °C, vapor patches are shown in Fig. 8(b) sliding along the heated surface, separated by liquid wetting fronts, but the overall thickness of the vapor layer is significantly smaller because of the strong condensation effects.

5.2. Void fraction estimation method

As shown in Fig. 8(a) and (b), the vapor generally appears very dark and the liquid white in the captured images. Based upon this strong contrast between the phases and thin rectangular cross-section of the channel,

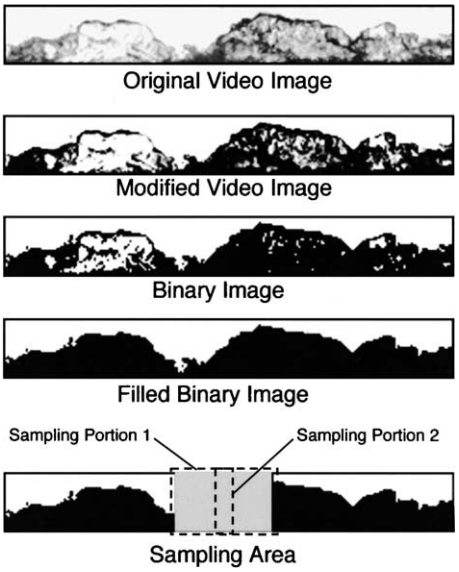

Fig. 9. Procedure for void fraction estimation.

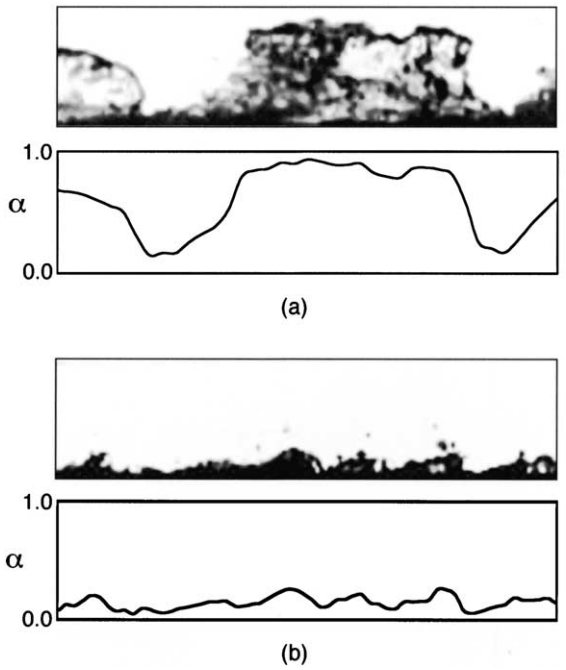

Fig. 10. Video image prior to CHF and calculated void fraction for (a) $\Delta T_{sub,o} = 3$ °C and (b) $\Delta T_{sub,o} = 30$ °C.

it is possible to use image analysis software to estimate the void fraction. Fig. 9 outlines the basic operations involved. The video images captured by the canon camera during the transient CHF tests were first downloaded into an image analysis program. The captured video images consist of 256 levels of gray-scale color. Image quality was first enhanced by increasing the contrast. The images were then converted to a two color binary image using a threshold operation. The threshold value was adjusted until the liquid–vapor interface in the binary image resembled that in the original image as closely as possible. Next the area below the liquid–vapor interface was filled black. This series of operations resulted in the vapor and liquid phases consisting of totally black and totally white areas, respectively.

To calculate void fraction, a portion of the image was selected which extended from the heated wall to the opposite wall of the channel, as shown in Fig. 9. The image analysis software estimates the void fraction as the area occupied by the black pixels (vapor) in the selected portion divided by the total area of the same portion. This calculation method was applied to many thousands of images in a video file using customized macro subprograms. A wide portion (sampling portion 1 in Fig. 9) was used to compute the overall trends of space-averaged void fraction. Void fraction estimation can be refined by using a thinner sampling portion. Fig. 10(a) and (b) illustrate the use of a thin sampling portion to generate void fraction, α, records. Notice both the small magnitude of α for subcooled flow and therefore far greater difficulty in interpreting void fraction trends compared to near-saturated flow.

Error associated with this void fraction estimation method comes in two forms. First, the method assumes that the flow is two-dimensional, meaning the vapor formations extend uninterrupted perpendicular to the camera viewing direction. These errors were minimized by both the rectangular cross-section and very short width (2.5 mm) of the flow channel. Secondly, there is some error associated with the threshold operation, since it is not possible to exactly duplicate the information contained in a 256 color image with a two color image and some of the small vapor bubbles entrained in the bulk liquid flow may not be accounted for.

6. Void fraction results

Fig. 11(a) shows the void fraction record from the last steady-state point before CHF to power cut-off after CHF for vertical upflow at $U = 1.5$ m/s and $\Delta T_{sub,o} = 3$ °C. Each second produces 30 void fraction data points. The void fraction was calculated at a location one-sixth the heated length from the downstream edge of the heater. A wide sampling portion was used to generate this plot, which causes some truncation of peak and trough values but effectively captures the overall trend of mean vapor layer thickness. Periodic rises and falls in void fraction, which are more evident in Fig. 9(a), are manifest in the form of data scatter about a void fraction mean.

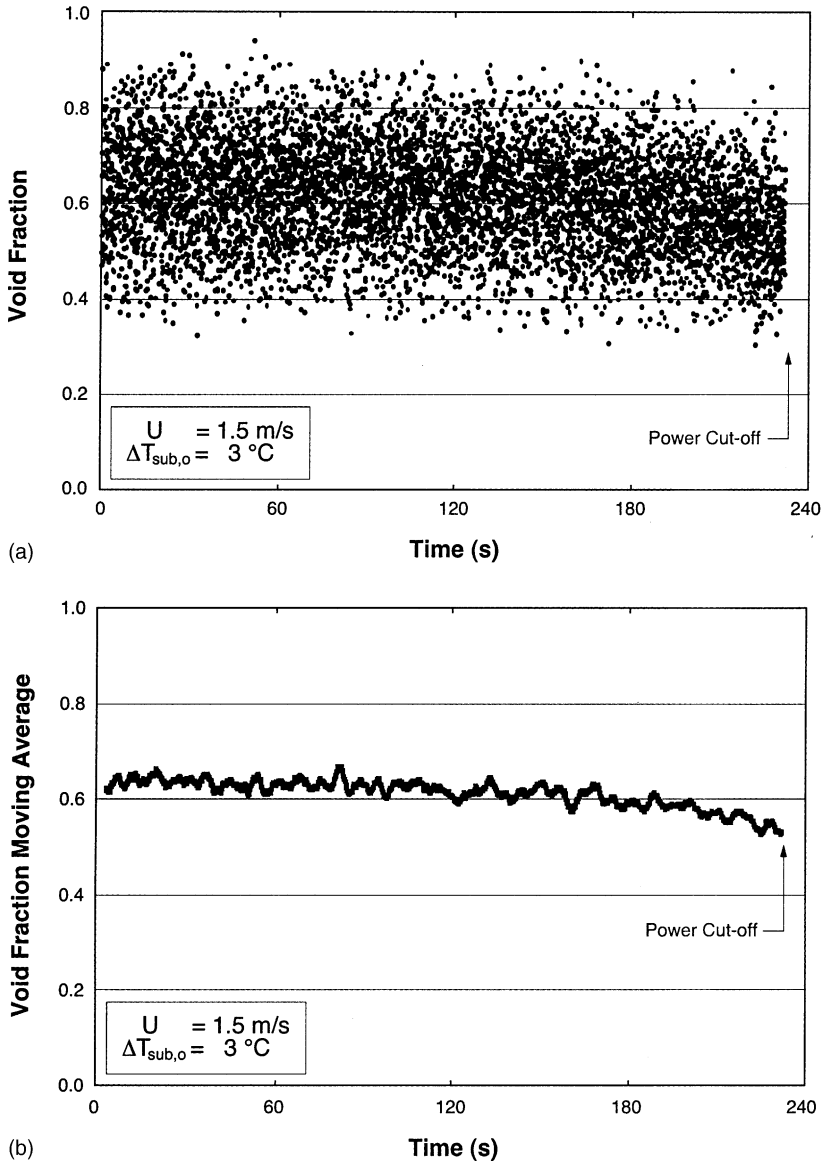

Fig. 11. Variations of (a) instantaneous void fraction and (b) void fraction moving average during CHF transient for vertical upflow at $U = 1.5$ m/s and $\Delta T_{sub,o} = 3$ °C.

Fig. 11(b) shows the moving average of the void fraction data shown in Fig. 11(a), which, for a particular time t, is defined as the average of the void fraction at that time and the 99 prior video images:

$$\bar{\alpha}(t) = \frac{1}{100}\sum_{i=0}^{99} \alpha(t - i \cdot \Delta t). \tag{7}$$

A key benefit of the moving average is its effectiveness at eliminating the data scatter and tracking the mean thickness of the wavy vapor layer.

Fig. 12(a) and (b) show plots of void fraction and void fraction moving average, respectively, for $U = 1.5$ m/s and $\Delta T_{sub,o} = 30$ °C. These two figures show significantly lower void fraction values compared to $\Delta T_{sub,o} = 3$ °C, Fig. 11(a) and (b), because of the appreciable reduction in net vapor generation in subcooled flow.

Interestingly, Fig. 11(a) and (b) show the vapor layer maintaining a somewhat constant mean vapor layer thickness during the CHF transient until the power cut-off point. A slight decrease in void fraction is detected as

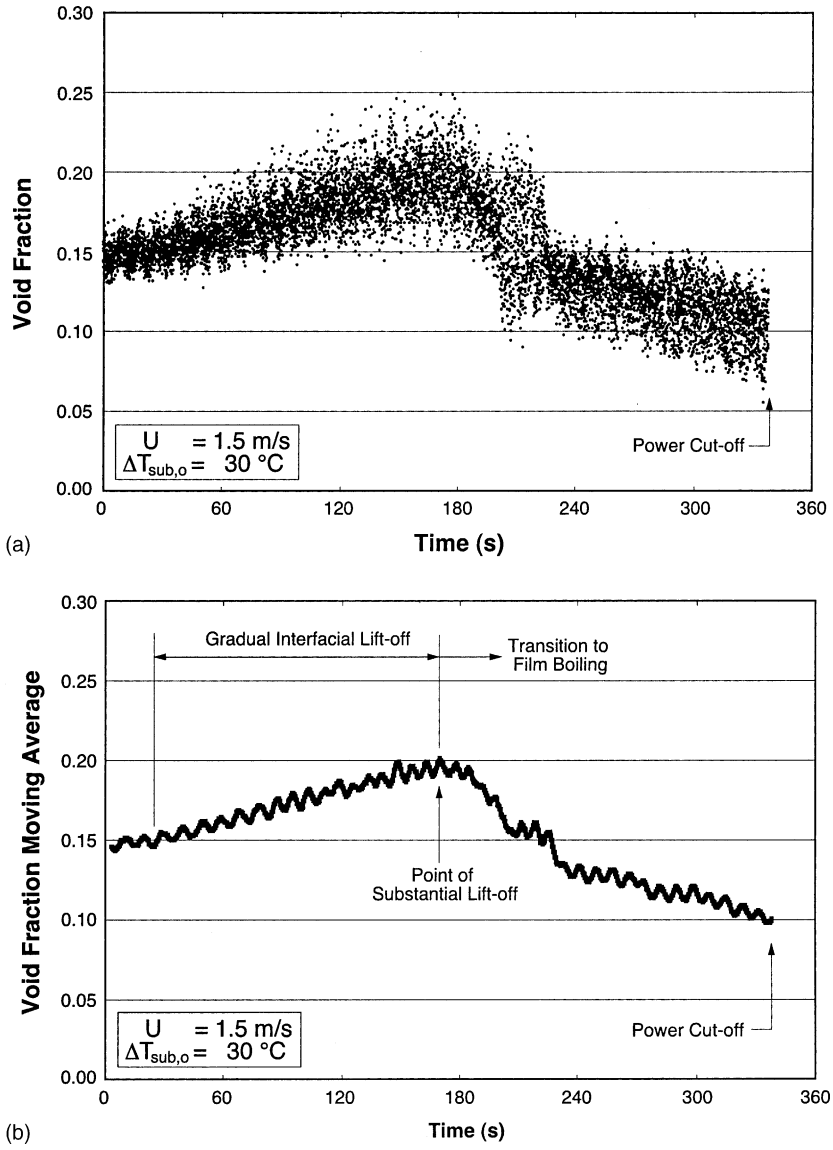

Fig. 12. Variations of (a) instantaneous void fraction and (b) void fraction moving average during CHF transient for vertical upflow at $U = 1.5$ m/s and $\Delta T_{sub,o} = 30$ °C.

the vapor layer begins to develop into a continuous vapor film.

Fig. 12(a) and (b) show the void fraction trend is far more drastic for $\Delta T_{sub,o} = 30$ °C. This is because small changes in the mean vapor layer thickness have an appreciable impact on a predominantly low void fraction (i.e., thin vapor layer) flow. This sensitivity is greatly diminished for $\Delta T_{sub,o} = 3$ °C where the overall void fraction values are very large to start with. Most notably, the void fraction records for $\Delta T_{sub,o} = 30$ °C can actually detect wetting front lift-off during the CHF transient quite well. The gradual initial increase in void fraction points to an increasing number of wetting fronts incurring lift-off. This process seems to reach some peak value (indicated in Fig. 12(b) as "point of substantial lift-off") before the vapor layer begins to thin down to a continuous vapor film.

Fig. 12(a) and (b) are the first strong evidence of the validity of the interfacial lift-off mechanism for subcooled flow boiling CHF. In fact, these figures provide a fairly detailed depiction of both the lift-off process and eventual transition to film boiling.

Future work should therefore focus on determining the partitioning of wall energy between sensible and la-

tent heat components to derive accurate energy balance framework in which to incorporate the interfacial lift-off model.

7. Conclusions

This study employed high-speed video imaging techniques and image analysis software to explore vapor layer formation during the transient that accompanied flow boiling CHF. While prior work by the authors and co-workers has demonstrated the effectiveness of the interfacial lift-off model at predicting CHF over broad ranges of velocity and flow orientation, these efforts were focused mostly on near-saturated conditions. Therefore, a key objective of this study was to ascertain the validity of the interfacial lift-off mechanism for subcooled flow boiling. Key findings from the study are as follows:

(1) The combination of video imaging of flow boiling in a thin rectangular channel and image analysis software is an effective means to estimating void fraction as well as tracking the wavy vapor layer development during the CHF transient.
(2) Video images and void fraction records of both near-saturated and subcooled flow show the development of a wavy vapor layer which propagates along the heated wall permitting cooling prior to CHF in wetting fronts corresponding to the wave troughs.
(3) The void fraction records for subcooled flow boiling show the CHF transient is accompanied by gradual lift-off of wetting fronts culminating in some maximum vapor layer mean thickness, following which the vapor layer begins to thin down as the transition to film boiling ensues.
(4) This study proves the interfacial lift-off model is equally valid for subcooled flow boiling CHF as it is for saturated. Future work should therefore focus on understanding the partitioning of wall energy between sensible and latent components to derive accurate energy balance framework in which to incorporate the interfacial lift-off model.

Acknowledgements

The authors are grateful for the support of the National Aeronautics and Space Administration under grant no. NAG3-2336.

References

[1] J.G. Collier, J.R. Thome, Convective Boiling and Condensation, third ed., Clarendon Press, Oxford, UK, 1994, pp. 325–424.
[2] S.S. Kutateladze, A.I. Leont'ev, Some applications of the asymptotic theory of the turbulent boundary layer, in: Proceedings of the Third International Heat Transfer Conference, New York, AIChE J. 3 (1966) 1–6.
[3] L.S. Tong, Boundary-layer analysis of the flow boiling crisis, Int. J. Heat Mass Transfer 11 (1968) 1208–1211.
[4] L.S. Tong, A phenomenological study of critical heat flux, ASME Paper 75-HT-68, 1975.
[5] J.C. Purcupile, S.W. Gouse Jr., Reynolds flux model of critical heat flux in subcooled forced convection boiling, ASME Paper 72-HT-4, 1972.
[6] J. Weisman, B.S. Pei, Prediction of critical heat flux in flow boiling at low qualities, Int. J. Heat Mass Transfer 26 (1983) 1463–1477.
[7] J. Weisman, S. Ileslamlou, A phenomenological model for prediction of critical heat flux under highly subcooled conditions, Fusion Technol. 13 (1988) 654–659.
[8] M.A. Styrikovich, E.I. Nevstrueva, G.M. Dvorina, The effect of two-phase flow pattern on the nature of heat transfer crisis in boiling, in: U. Grigull, E. Hahne (Eds.), Heat Transfer 1970: Fourth International Heat Transfer Conference, Paper B 6.10, vol. 6, Elsevier Publishing Co., Amsterdam, Netherlands, 1970.
[9] M.P. Fiori, A.E. Bergles, Model of critical heat flux in subcooled flow boiling, in: U. Grigull, E. Hahne (Eds.), Heat Transfer 1970: Fourth International Heat Transfer Conference, Paper B 6.3, vol. 6, Elsevier Publishing Co., Amsterdam, Netherlands, 1970.
[10] R. Mesler, A mechanism supported by extensive experimental evidence to explain high heat fluxes observed during nucleate boiling, AIChE J. 22 (1976) 246–252.
[11] S.B. van der Molen, F.W.B.M. Galjee, The boiling mechanism during burnout phenomena in subcooled two-phase water flows, in: Heat Transfer 1978: Sixth International Heat Transfer Conference, vol. 1, Hemisphere Pub. Corp., Washington, DC, 1978, pp. 381–385.
[12] G.P. Celata, M. Cumo, A. Mariani, G. Zummo, Preliminary remarks on visualization of high heat flux burnout in subcooled water flow boiling, in: G.P. Celata, R.K. Shah (Eds.), Two-Phase Flow Modelling and Experimentation 1995, vol. 2, Edizioni ETS, Pisa, Italy, 1995, pp. 859–866.
[13] C.H. Lee, I. Mudawar, A mechanistic critical heat flux model for subcooled flow boiling based on local bulk flow conditions, Int. J. Multiphase Flow 14 (1989) 711–728.
[14] W.-S. Lin, C.-H. Lee, B.-S. Pei, An improved theoretical critical heat flux model for low-quality flow, Nuclear Technol. 88 (1989) 294–306.
[15] Y. Katto, A physical approach to critical heat flux of subcooled flow boiling in round tubes, Int. J. Heat Mass Transfer 33 (1990) 611–620.
[16] Y. Katto, Prediction of critical heat flux of subcooled flow boiling in round tubes, Int. J. Heat Mass Transfer 33 (1990) 1921–1928.
[17] Y. Katto, A prediction model of subcooled water flow boiling CHF for pressure in the range 0.1–20 MPa, Int. J. Heat Mass Transfer 35 (1992) 1115–1123.
[18] G.P. Celata, M. Cumo, A. Mariani, M. Simoncini, G. Zummo, Rationalization of existing mechanistic models

for the prediction of water subcooled flow boiling critical heat flux, Int. J. Heat Mass Transfer 37 (1994) 347–360.
[19] G.P. Celata, M. Cumo, Y. Katto, A. Mariani, Prediction of the critical heat flux in water subcooled flow boiling using a new mechanistic approach, Int. J. Heat Mass Transfer 42 (1999) 1457–1466.
[20] J.E. Galloway, I. Mudawar, CHF mechanism in flow boiling from a short heated wall—I. Examination of near-wall conditions with the aid of photomicrography and high-speed video imaging, Int. J. Heat Mass Transfer 36 (1993) 2511–2526.
[21] J.E. Galloway, I. Mudawar, CHF mechanism in flow boiling from a short heated wall—II. Theoretical CHF model, Int. J. Heat Mass Transfer 36 (1993) 2527–2540.
[22] C.O. Gersey, I. Mudawar, Effects of heater length and orientation on the trigger mechanism for near-saturated flow boiling critical heat flux—I. Photographic study and statistical characterization of the near-wall interfacial features, Int. J. Heat Mass Transfer 38 (1995) 629–641.
[23] C.O. Gersey, I. Mudawar, Effects of heater length and orientation on the trigger mechanism for near-saturated flow boiling critical heat flux—II. Critical heat flux model, Int. J. Heat Mass Transfer 38 (1995) 643–654.
[24] J.C. Sturgis, I. Mudawar, Critical heat flux in a long, rectangular channel subjected to one-sided heating—I. Flow visualization, Int. J. Heat Mass Transfer 42 (1999) 1835–1847.
[25] J.C. Sturgis, I. Mudawar, Critical heat flux in a long, rectangular channel subjected to one-sided heating—II. Analysis of critical heat flux data, Int. J. Heat Mass Transfer 42 (1999) 1849–1862.
[26] H. Zhang, I. Mudawar, M.M. Hasan, Experimental assessment of the effects of body force, surface tension force and inertia on flow boiling CHF, Int. J. Heat Mass Transfer 45 (2002) 4079–4095.
[27] H. Zhang, I. Mudawar, M.M. Hasan, Experimental and theoretical study of orientation effects on flow boiling CHF, Int. J. Heat Mass Transfer 45 (2002) 4463–4477.